IEEE Transactions on Information Forensics and Security, vol. 4, no. 1, pp. 98-110, March. 2009

Personal Authentication using Finger Knuckle Surface

Ajay Kumar, Ch. Ravikanth

This paper investigates a new approach for personal authentication using finger back surface imaging. The texture pattern produced by the finger knuckle bending is highly unique and makes the surface a distinctive biometric identifier. The finger geometry features can be simultaneously acquired from the same image, at the same time and integrated to further improve the user identification accuracy of such system. The finger back surface images from each of the users are normalized to minimize the scale, translation and rotational variations in the knuckle images. This paper details the development of such an approach using peg-free imaging. The experimental results from the proposed approach are promising and confirm the usefulness of such approach for personal authentication.

1. Introduction

The rapid growth in the use of e-commerce applications and penetration of information technology into the daily life requires reliable user identification for effective and secured access control. The hand-based biometrics has received considerable attention in recent years which exploits several internal and external features that are quite distinct in an individual. The user-acceptance for hand-based biometrics system is very high. These systems are becoming more convenient and user-friendly with the introduction of peg-free and touchless imaging. The usage of these hand-based systems for large scale personal authentication requires further efforts to explore additional features that can be simultaneously extracted from the hand images. In this work our efforts are focused to develop an automated method to extract knuckle texture and geometrical features from finger-back surface and investigate its performance for a potential biometric system.

1.1 Related Work

The hand-based biometrics has attracted lot of attention and personal identification using palmprint [1]-[2], [4]-[6], [14]-[15] hand-geometry, [7]-[8], 3D finger-geometry [9]-[10], and

hand vein [11]-[13] have been proposed in the literature. The earlier approaches achieved the results by constraining the position and posture of hands by using pegs [2], [8], [11]. However, such approaches presented inconvenience and difficulties for some user groups especially the children and elderly. Therefore a lot of emphasis has been laid on touchless and peg-free image acquisition [4], [10], [12], [16] [38]. The peg-free imaging, although highly convenient to users, generates images with more rotational and scale changes. Therefore the efforts are further required to improve the reported performance [14], [16].

The finger surface posses unique patterns that have been utilized in the personal identification [9]-[10]. Woodard and Flynn [9] have examined the fine features of finger surface for its use in biometric system. Authors have presented promising results using curvature and shape-based index from finger surface features extracted from 3D range images. However, the work detailed in [9] does not exploit the texture information that can be simultaneously extracted from the intensity images of hands. Malassiotis *et al*. [10] have also illustrated the utility of 3D finger geometry features using peg-free imaging. This approach has illustrated promising results while combining the color and 3D information to authenticate user hands in the cluttered background. The finger shape information is generally believed to be less discriminative and only suitable for small scale user identification. The limited number of cross sectional 3D measurements and absence of any finger texture information in [10] poses further limitations on the scalability of this approach for its real usage. Ribaric and Fratric [5], [35] employed appearance based features from the finger and palm surface images for the personal identification. However, the authors in [5], [35] have employed scanner for imaging which is very slow and hence not suitable for online user authentication. Also, in [5] the geometrical features from the acquired images were not utilized which could offer further performance improvement [35] when utilized in conjunction with palm texture features. The work detailed in [5], [35] is promising but it relies on crease and wrinkle details on the palm-side of fingers which are quite limited. The anatomy of fingers allows them to bend in forward (palm-side)

direction and resist backward motion. This asymmetry results in very limited amount of crease and wrinkles on the palm-side of the fingers.

1.2 Motivation

The anatomy of human hand is quite complicated and closely related to the medicine and other branches of biology. The finger-back surface, also known as dorsum of hand, can be highly useful in user identification and has not yet attracted the attention of researchers. The image pattern formation from the finger-knuckle bending is highly unique and makes this surface a distinctive biometric identifier. The finger geometry features can be acquired from the same image, at the same time and integrated to improve the performance of the system. The peg-free imaging of the finger back surface is highly convenient to users. Such images can be acquired online and used to extract scale, translation and rotational invariant knuckle features for user authentication.

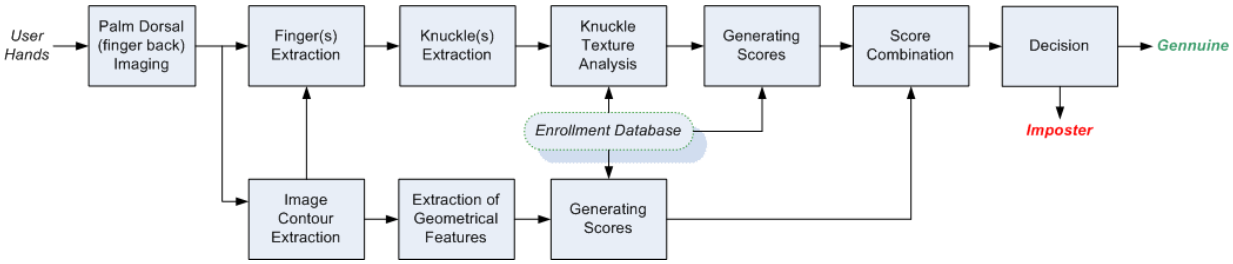

Figure 1: Block diagram of the personal authentication using finger-back surface.

1.3 Proposed System

In this paper, a new user authentication system using finger-back surface imaging is investigated. The proposed system employs peg-free imaging and develops a robust approach adapted to the resulting hand-pose variations and problems due to the appearance of the rings. An important aspect of our approach is the simultaneous extraction of finger-geometry features which are employed to achieve further performance improvement. The block diagram of the proposed approach is shown in figure 1. The details of the imaging setup are provided in section 2.1. The image contours extracted from the acquired images are used for image normalization and the extraction of region of interest (ROI) is detailed in section 2.2 while the

extraction of finger geometry features is detailed in section 3-4. The automated extraction of four hand fingers and then the knuckle region images is illustrated in section 5. This section also considers two different methods of extracting knuckle regions and details the problem due to finger rings. The analysis of knuckle texture images using appearance-based techniques is detailed in section 6 which includes the details on the combination of matching scores from four knuckles. The experiments and results from this work are summarized in section 7. This section also includes discussion on performance analysis and the key comparisons. Finally, the main conclusions from this paper are summarized in section 8.

(a) (b)

Figure 2: Image acquisition setup in (a) and acquisition of a sample finger back image in (b)

2. Image Acquisition and Preprocessing

2.1 Image Acquisition

An acquisition system has been developed for the collection of finger-back images as there is no public database available to date for such images. A very user-friendly, peg-free imaging system is constructed and shown in figure 2. This imaging system uses a digital camera focused against a white background under uniform illumination. The camera has been set and fixed at a distance of 20 cm from the imaging surface. Non-uniform illumination cast shadows and reflections at the hand boundaries which significantly reduces the performance. Therefore, the image acquisition is uniformly illuminated by a fixed light source above the hand. The resolution of the acquired image is 1600 × 1200 pixels. Each subject is requested to place the hand on the support with their back hand facing the sensor. The subject can visualize the

placement of their hand from the live-feedback on small plasma display. The acquisition of a sample image is shown in figure 2(b). The prior work on hand-based biometric identification [4]-[5], [8] used black background during the image acquisition. However, the white background is chosen in our imaging. The reason is that the finger back texture is often dark and requires relatively simpler pre-processing as compared to with those images acquired with dark background.

2.2 Preprocessing

Each of the acquired hand images are firstly subjected to thresholding operation to obtain the binarized image. The magnitude of thresholding limit η is computed by maximizing the

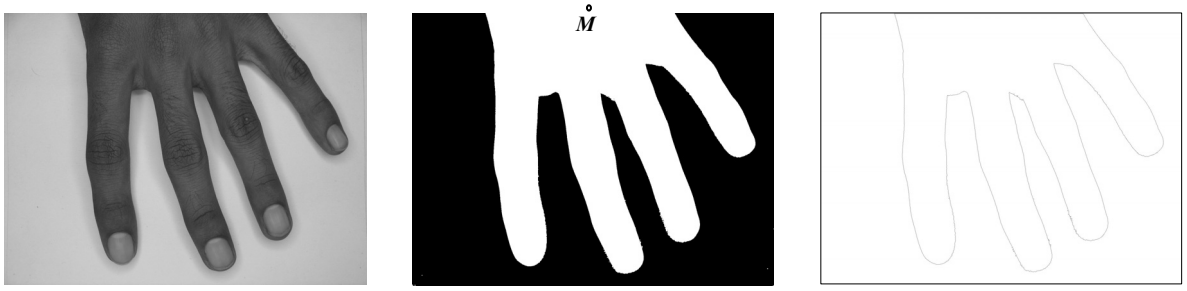

(a) (b) (c)

Figure 3: The acquired image in (a), binarized image in (b), and the extracted contour image in (c)

object function $J_{op}(\eta)$, which denotes the measure of separablity between the two classes of pixels in the image;

$$J_{op}(\eta) = \frac{P_1(\eta)P_2(\eta)[\mu_1(\eta) - \mu_2(\eta)]}{[P_1(\eta) + P_2(\eta)]} \tag{1}$$

where the numbers of pixels in class 1 and 2 are represented by $P_1(\eta)$ and $P_2(\eta)$, $\mu_1(\eta)$ and $\mu_2(\eta)$ are the corresponding sample mean [17]. The resulting binarized image contains small sporadic dots that generate spurious results in the extraction of finger geometry features. These spurious pixels are also observed due to the hairs at the finger boundaries. Therefore morphological erosion operation using a 3 × 3 structuring element is employed on the binarized images to remove sporadic dots. This operation also helps to smoothen the image contour. Then the boundary of the resultant image is extracted using contour tracing (figure

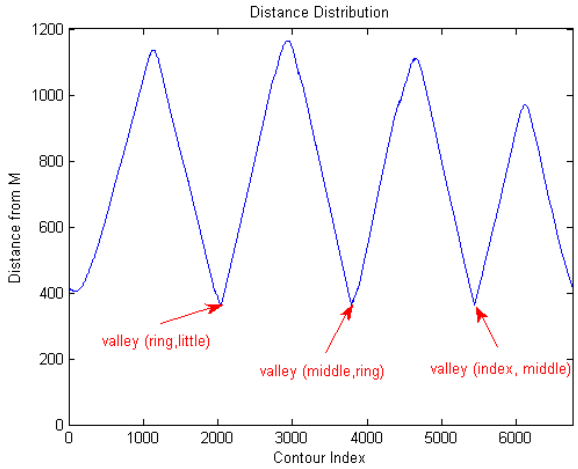

Figure 4: Distribution of the contour distances from the center point *M*

3-c). Even after removing small contours, we ensure that correct contour boundary is extracted by employing only the largest possible contour in the image because hand contour is the largest contour.

3. Locating Fingers

The contour pixels, as shown in figure 3(c), from the shape boundary are stored in a vector named as B_{PV} (Border Pixel Vector). The midpoint of the palm-wrist is marked as *M* (figure 3-b) and used for image normalization. The Euclidean distances between the B_{PV} points and *M* are computed and resulting distance distribution diagram is illustrated in figure 4. The pattern in the distance distribution (figure 4) is quite similar to the shape of the hand. The local minima correspond to the valleys of the hand. The extreme base points of the hands, shown as *E1* and *E2* in figure 5, are located from the shortest distance of the pixel in the contour of the image

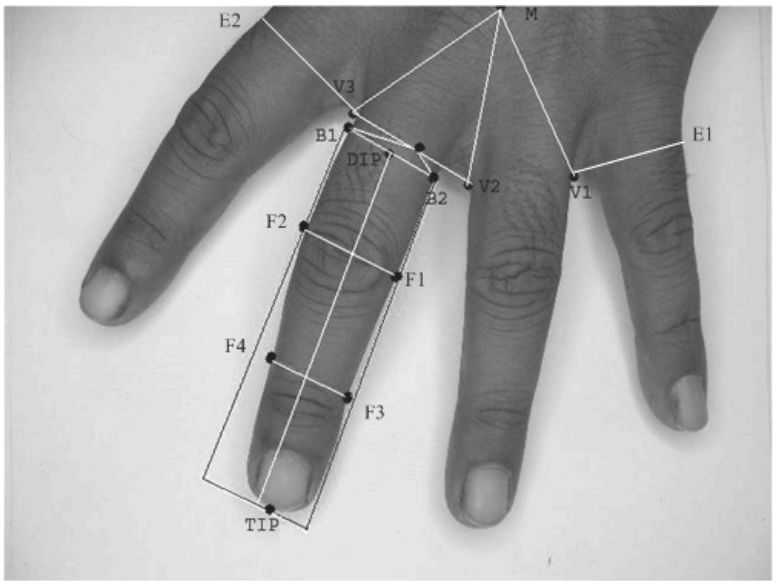

Figure 5: Prominent finger points for finger geometry feature extraction

from the adjacent valley points. Therefore the point *E2* is located by calculating the shortest distance from *V3* (located from the contour distance in figure 4) among the first few B_{PV} points. Similarly, the point *E1* is located using *V1*. The initial dip points are computed as the mid point of these valley points. Thus for the middle finger shown in figure 5, the initial dip point is estimated as mid point of *V2* and *V3* (marked as dot). Next, the base points of each of the fingers (*B1* and *B2*) are determined from the points of B_{PV} which are at minimum distance from the initial dip point of that corresponding finger. The dip point of the finger is updated as the midpoint of the base points of the finger and shown as DIP in figure 5 for the middle finger. Next the contour pixels between the base points of the finger are divided into 6 parts for the calculation of widths. The mid point of the base points along the border of the finger is marked as the finger tip.

4. Finger Geometry Features

The finger geometry parameters extracted from the hand images in the previous section are employed to locate the gray-level pixels belonging to the four individual fingers. The located finger pixels are used to extract the knuckle regions for feature extraction. Firstly, four additional points are located from the finger contour. Two of them are at one-third of the distance between the fingertip and the base points of the finger and the other two at the two-third distance (*F1*, *F2*, *F3*, and *F4* in figure 5). The line joining the middle points of the line segments *F1-F2* and *F3-F4* defines the line of symmetry of the finger-strip region. The length of the strip is chosen to be the length of the finger. The width of the strip is chosen to be the minimum distance between the base points of the finger (*B1-B2*). With this length and width, the ROI pixels for each of the four fingers are extracted symmetrically on both sides of the symmetry line. A total of six finger geometry features are computed from each of the fingers resulting in a total of 24 finger geometry features. These include one finger length, three finger widths, finger perimeter, finger area, and summarized as follows:

• *Finger Length*: The finger length is estimated as the distance between the finger tip and the midpoint of the base points of the finger (referred here as dip point). The distance between TIP and DIP in figure 5 denotes the finger length.

• *Finger Width*: Three finger widths are estimated as shown in the figure 5. The finger contour is partitioned into six equal segments and the distance between the intermediate points are estimated as finger widths. The three finger widths *w1*, *w2*, and *w3* are estimated from acquired images as follows:

$$w1 = dist(B1,B2),\ w2 = dist(F1,F2),\ w3 = dist(F3,F4) \quad (2)$$

• *Perimeter*: The perimeter is estimated as the number of pixels on the contour of the finger.

• *Area*: The number of pixels covered within the contour of the finger are computed and estimated as the finger area.

4.1 Normalization

The normalization of extracted geometrical features is essential because their varying ranges and order, *e.g.*, the magnitude of the estimated finger area is significantly larger as compared to the finger widths. Several feature normalization techniques have been detailed in the literature

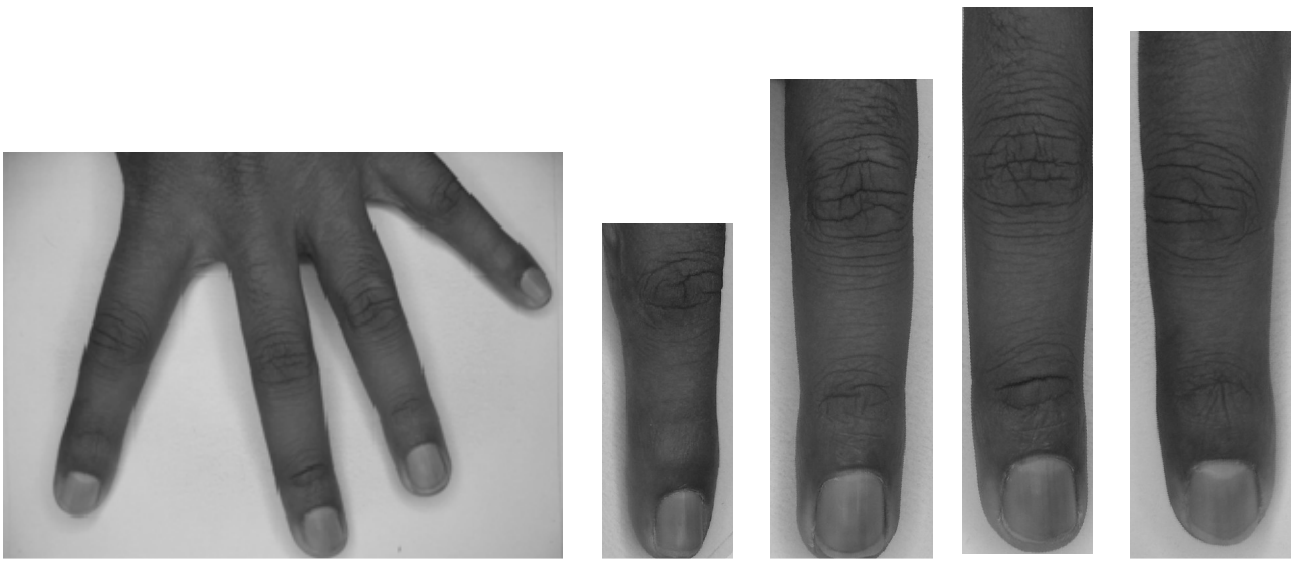

(a) (b) (c) (d) (e)

Figure 6: The acquired image (a) and the fingers extracted, (b) little, (c) ring, (d) middle, and (e) index finger.

[18]. We considered two computationally simpler normalization schemes to obtain the normalized feature vector x'_{ik}.

- Min-Max Normalization:

$$x'_{ik} = \frac{x_{ik} - \min(x_{ik})}{\max(x_{ik}) - \min(x_{ik})} \tag{3}$$

where $x_{ik} = \{x_{i1}, x_{i2}, \ldots, x_{iN}\}$ is the feature vector with N values and x'_{ik} is the corresponding normalized feature vector.

- Z-Score Normalization:

$$x'_{ik} = \frac{x_{ik} - \alpha}{\beta} \tag{4}$$

where α and β are the mean and variance of the corresponding feature. It was observed that Min-Max normalization achieves better performance than Z-Score normalization for our approach. The comparative performance from geometrical features using two normalization schemes considered are provided in section 7.

5. Extraction of Knuckles

Once the finger regions are segmented, the knuckle regions are located for the extraction of reliable features. Figure 6 shows the four fingers extracted from a typical acquired hand image. It may be noted that the finger images extracted from each of the hand images are of varying

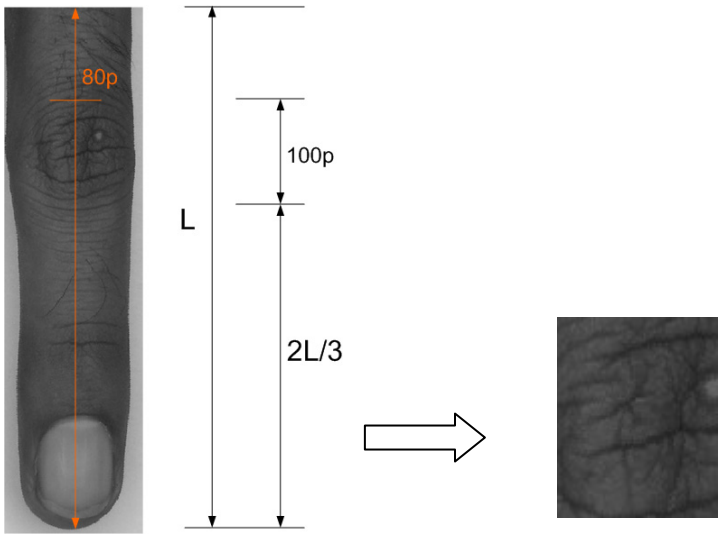

(a) (b)

Figure 7: Method A: Extracted finger from acquired image (a) and corresponding Knuckle region obtained.

sizes. We investigated two methods for extracting knuckle regions from the segmented fingers.

(1) *Method A*: In this approach a fixed size knuckle region of the finger is extracted based on the finger length. For example, along the central line of the finger, a region of fixed size 80 × 100 pixels is extracted symmetrically from the middle finger at a distance of one-third of the length from the tip of the finger as shown in figure 7. Similarly, a region of 50 × 100 pixels is extracted from little and index fingers while a region of 80 × 100 is extracted from ring finger.

(2) *Method B*: Another method was investigated to further improve the localization of the region of interest. The Canny edge-detector is firstly applied on the extracted finger image. The density of the high intensity pixels in the resultant image is used for ROI extraction. As can be seen in figure 8, in the knuckle region the high intensive pixels' density is very high. This region can be centrally extracted on either side of the central line as is the case with the previous method. Therefore a 80 × 100 pixel highly dense region, *i.e*. region with most edge elements along finger symmetry line, is extracted centrally from the base part of the finger. In a similar manner, fixed regions of size 50 × 100 pixels are extracted from little and index fingers.

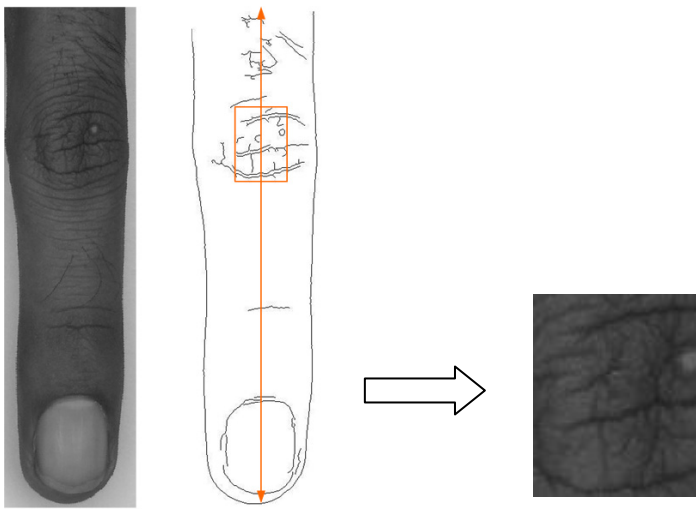

(a) (b) (c)

Figure 8: Method B: Finger image (a), corresponding image after edge detection (b), and the extracted knuckle (c).

5.1 Analysis of two Methods

The two methods considered above extract a fixed size knuckle ROI from the fingers of

(a)

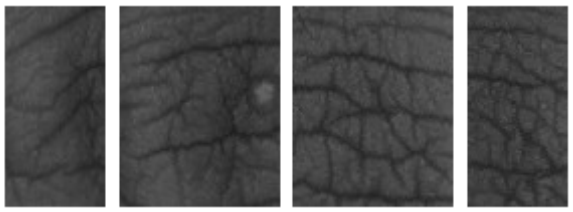

(b)

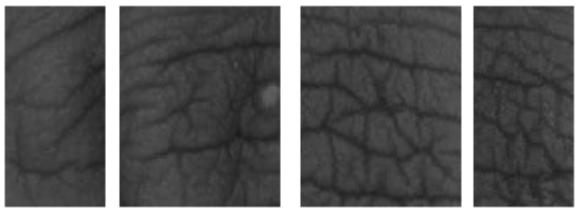

(c)

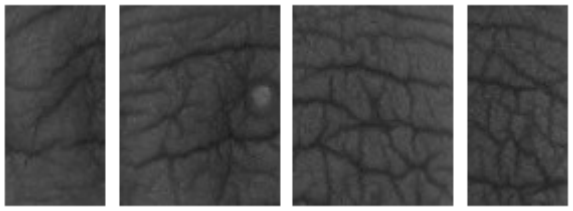

(d)

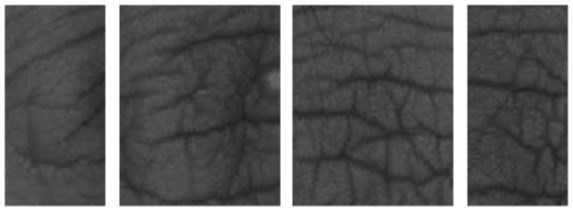

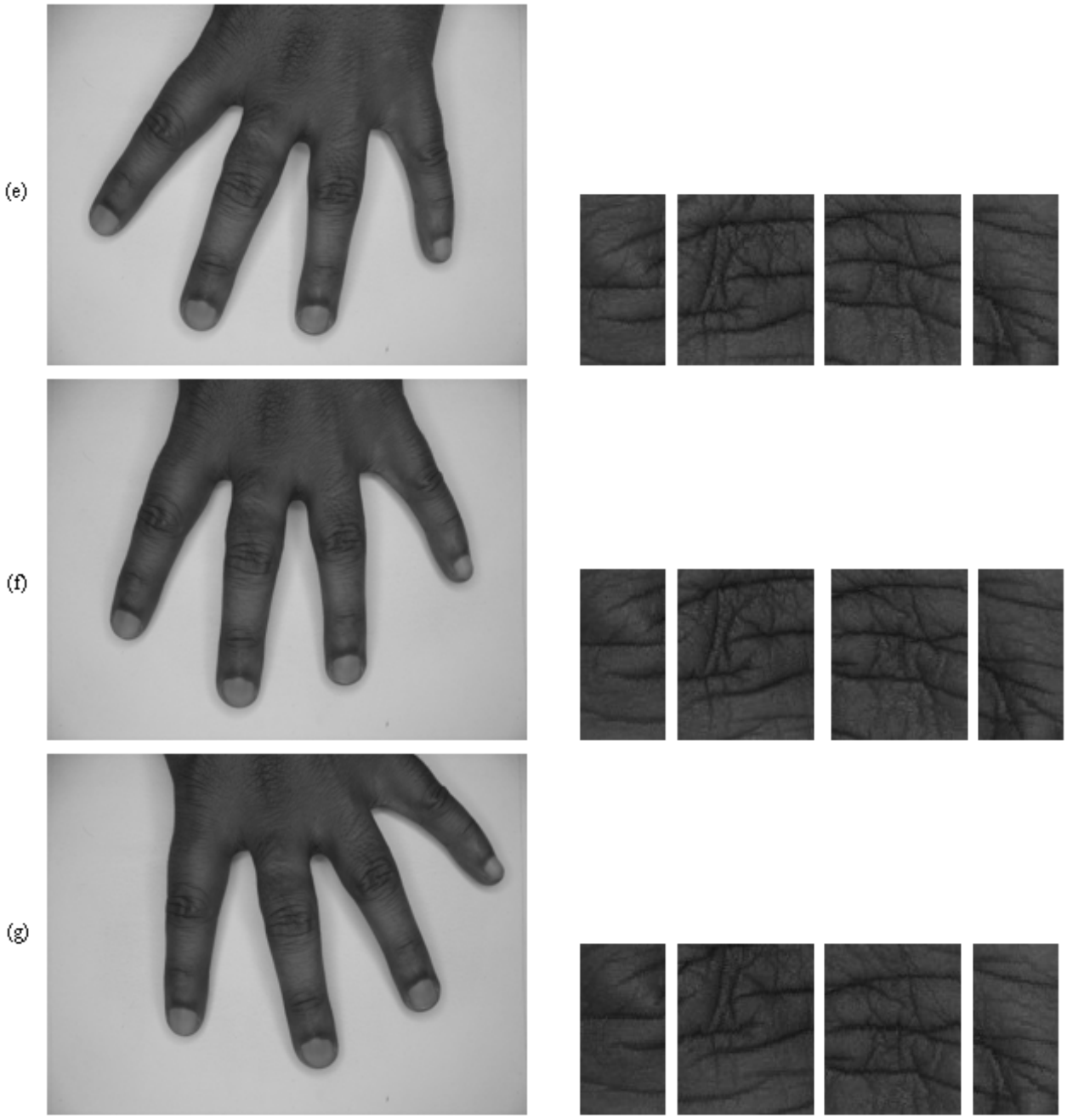

Figure 9: Automated extraction of four finger knuckles from the acquired images in (a)-(g)

varying sizes. These methods are observed to be quite robust to rotation and translation variations of the fingers in the acquired hand image. Figure 9 shows the different set of knuckle regions extracted from the acquired images with varying position using method B. These results suggest that our approach of automatically extracting the knuckle regions has been highly effective. This can also be ascertained from figure 10 that shows the knuckles extracted from an image, which is a part of the database, even with the high rotation of the presented

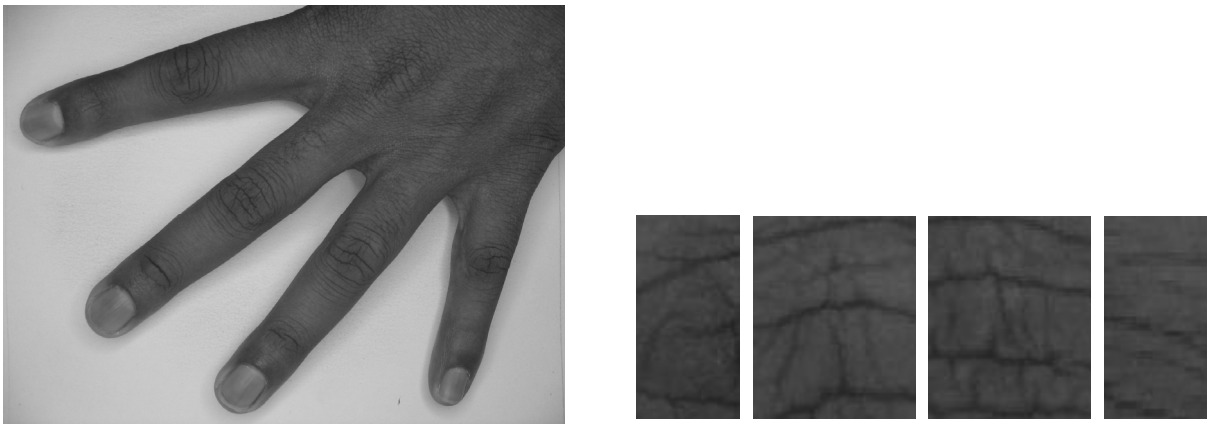

Figure 10: One of the poor samples of the rotated image from our database and the extracted knuckle samples

hand during image acquisition. Comparatively, method A produces less accurate localization as compared to method B primarily because the extracted fingers are not of fixed size. On the other hand, method B suffers from the sensitivity of empirically determined threshold values for edge-detection. Also the presence of ring-bearing fingers extremely affects the localization accuracy as shown in figure 11. The problem due to the rings is eliminated by firstly detecting the presence of rings from their extremely high shiny (thereby high pixel intensity value) surface. The pixel intensities along the center of extracted finger, (top and central region) are counted and compared with a threshold to detect the presence of ring. The summation plot of pixel intensities along the row of the image is shown in figure 12 and illustrates the ring detection. Once a ring is detected, the fixed knuckle region is extracted from the rest of the finger following the detected ring.

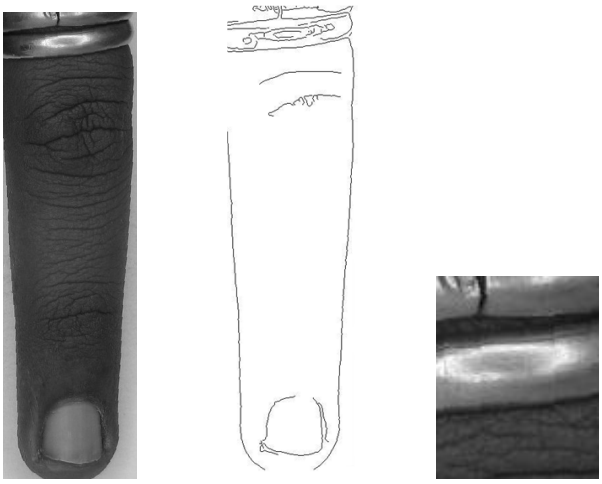

Figure 11: Image sample with ring and corresponding knuckle image (method B) without ring detection module.

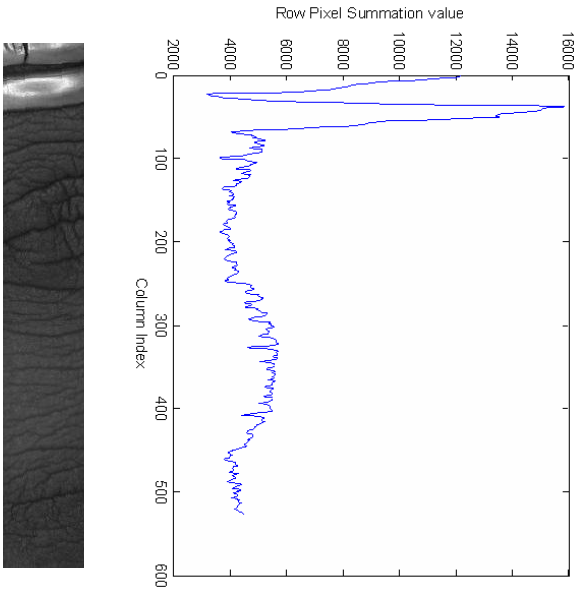

Figure 12: Two examples in (a) and (b) showing the ring bearing fingers and their summation plots.

6. Matching Knuckle Images

The knuckle images present a random texture which is observed to be quite unique in each of the user. The information content from the extracted knuckle image consists of certain local and global features which are observed to be quite stable. This information from knuckle images can be extracted by registering the variations in a ensemble of knuckle images, independent of any judgment of creases or lines. This information can then be used to authenticate individual users. In this work we considered three appearance-based approaches for generating matching scores from the knuckle images.

6.1 Principal Component Analysis

The principal component analysis (PCA) determines the basis vectors spanning an optimal subspace such that the mean square error between the projection of the training images onto this subspace and the original images is minimized. We call this set of optimal basis vectors as *eigenknuckles* since these are simply the eigenvectors of the covariance matrix computed from the vectorized images in the training set. The feature extraction steps begins with firstly representing each of the $N \times M$ pixel knuckle image by a vector and then computing its covariance matrix of these normalized vectors Θ_j as follows:

$$\Omega = \frac{1}{C}\sum_{j=1}^{C}\Phi_j\Phi_j^T \tag{5}$$

The computation of eigenvectors of $N*M \times N*M$ covariance matrix Ω is cumbersome due to the memory and computational constraints. Therefore the simplified method implemented in [32] is employed. The set of projection coefficients for each of the training knuckle images, from the set of *eigenknuckles*, is computed during training phase and employed for generating matching scores for test images.

6.2 Linear Discriminant Analysis

The Linear Discriminant Analysis (LDA) is defined by $Y=W_{opt}^T X$ where the columns of the W_{opt} matrix are the eigenvectors of $S_w^{-1}S_b$. The columns of W_{opt} are the orthonormal vectors. The matrices S_w and S_b are computed through the following equations [20]:

$$S_W = \sum_{j=1}^{C}\sum_{i=1}^{M}(X_{ij}-\mu_j).(X_{ij}-\mu_j)^T, \qquad \mu_i = \frac{1}{M_i}\sum_{j=1}^{M_i}X_{ij} \tag{6}$$

$$S_B = \sum_{j=1}^{C}M_i(\mu_j-\mu).(\mu_j-\mu)^T, \qquad \mu = \frac{1}{C}\sum_{i=1}^{C}\mu_i \tag{7}$$

This transformation is strongly effected by the number of classes (C), the number of samples (M), and the original space dimensionality (d). The number of training images is much smaller than the number of pixels in the knuckle images which often results in the singularity of S_w matrix. In order to avoid this, firstly, an intermediate transformation (PCA) is applied to reduce the dimensionality of the image space. In summary, the LDA searches for those vectors in the underlying space that best discriminate among classes (rather than those that best describe the data).

6.3 Independent Component Analysis

The subspace techniques that can create spatially localized features are receiving increasing attention in the literature [20]-[21]. Such techniques are expected to be more tolerant to the occlusion as the localized features help to implement region-based identification. The independent component analysis (ICA) is the most common subspace method of generating

spatially localized features. The goal is to find a linear representation of non-Gaussian data so that the components are statistically independent and not just linearly decorrelated like PCA. The key principle of ICA estimation is the non-Gaussianity [36]. The connection between the independence and non-Gaussianity is explained by central limit theorem. This theorem states that distribution of sum of *i.i.d.* (independent identically distributed) random variables tend to be more Gaussian than any of the original ones. In summary, higher is the independence among sources if their distributions have more non-Gaussianity. A quantitative measure of non-Gaussianity is required for its use in ICA estimation. The cumulant-based measures like kurtosis or entropy-based measures like negentropy are classically used for such measurement. The ICA representations have shown to capture the essential feature of the data. This approach can be viewed as if the eigenvectors of PCA are replaced by the independent source vectors in ICA. The ICA decomposition detailed in [22]-[23], [33] provides rapid convergence and was employed to extract basis vectors from the learning data.

6.4 Score Generation

The choice of subspace distance metric highly influences the performance and is empirically determined. In this work, the Euclidean distance metric was found to be most effective and used to generate the distance between the projection coefficients from training and test images. The matching scores obtained from the three individual sub-space methods (PCA, LDA, ICA) can also be combined to further improve the performance. The fusion of matching scores from these subspace methods has shown to offer effective performance improvement in the identification of human faces [24]-[26]. In this work the matching score combination using fixed fusion rules was employed as they are computationally simple. The combined matching score for every user i, $\forall\ i = 1, 2, \ldots C$, using SUM and PROD rule is quite effective and obtained as follows:

$$m_a(i) = \frac{1}{Z}\sum_{j=1}^{Z} s_{ij} \tag{8}$$

$$m_p(i) = \left(\prod_{j=1}^{Z} s_{ij} \right)^{\frac{1}{Z}} \quad (9)$$

where s_{ij} is the individual matching score from i^{th} user using j^{th} classifier, *i.e.*, sub-space method, $m_a(i)$ and $m_p(i)$ represents the consolidated matching scores using SUM and PROD rule respectively. In addition to the SUM and PROD rule, one can also combine the two sub-space methods using SUM rule and then use the PROD rule to further consolidate the resulting matching score with the score from third sub-space method. We refer such combination as the product of sum (POS) in this paper and is also investigated for performance improvement.

7. Experimental Results

The performance of the user authentication approach detailed in previous sections was evaluated on the real biometric data. Since there is no publicly available finger-back surface image database, to the best of our knowledge, we have to acquire the database of hand images for performance evaluation. The acquisition system constructed (figure 2) was used to collect the finger-back image database. The database was collected over a period of seven months, in two phases, with an average interval of about four weeks. The database of finger-back images from male and female subjects in the age group of 18-60 years from various ethnic groups was acquired. The majority of data was collected from the adults between age group of 20-25 years. The users were requested to keep the fingers wide open while imaging. A live display is provided for them to view the position of the hand. They were asked to change the orientation of the hand freely. No restriction is imposed on wearing of rings on one or more fingers and therefore the database has several images from users with rings. We acquired four images during the first phase and two images in the second phase. The database from 105 users with 630 images was used for the experimental evaluation.

The rigorous experiments were conducted to ascertain the best possible performance on

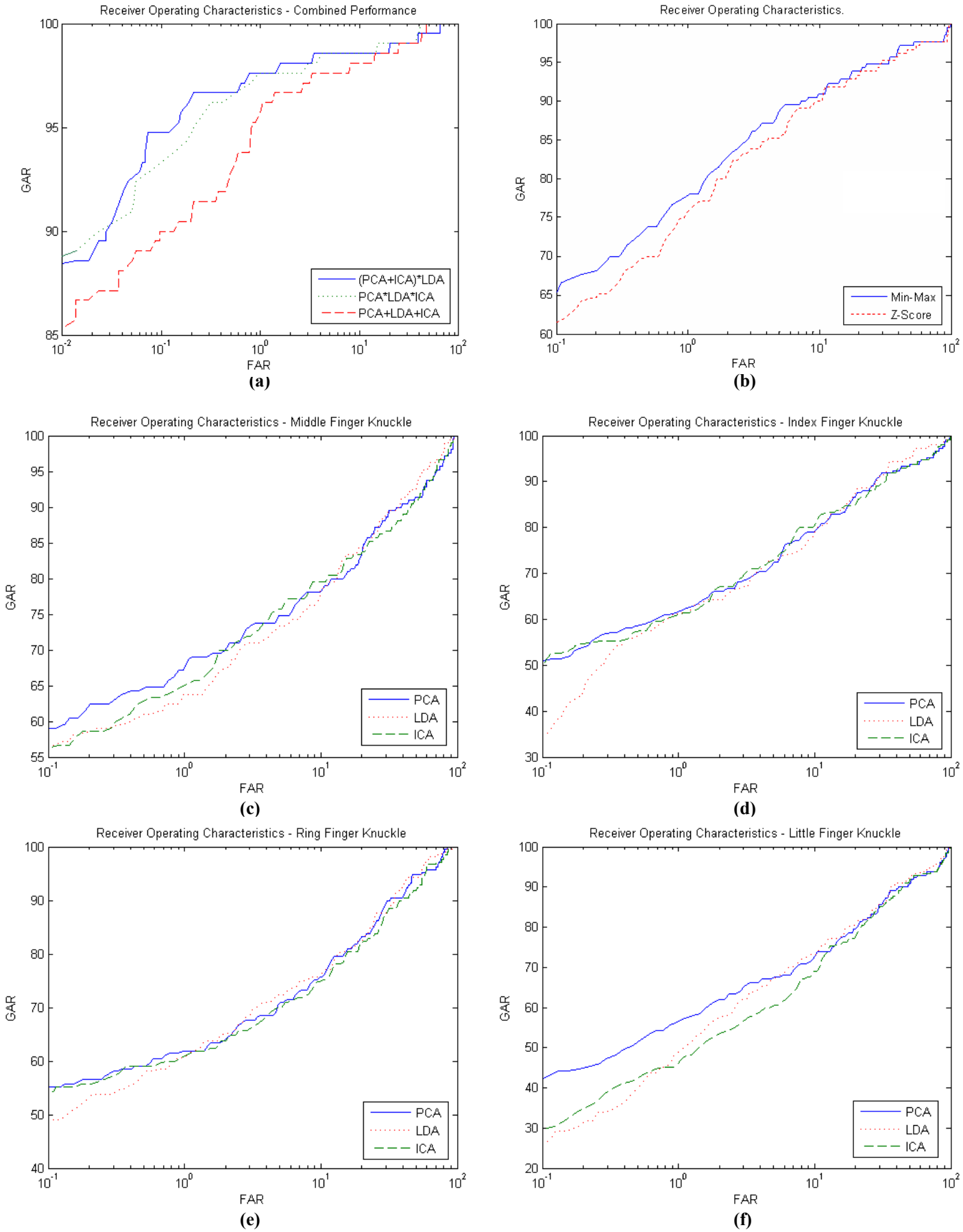

Figure 13: The ROC plots for combined performance in (a), finger geometry features in (b), middle, index, ring and little finger in (c), (d), (e) and (f) respectively.

Table 1: The GAR values at different values of FAR for various combinations

S. No.	Combination	GAR (%)		
		FAR = 0.1%	**FAR = 1%**	**FAR = 2%**
1	$\sum P_i$	79	88	89.5
2	$\prod P_i$	87.5	92	92.5
3	$\sum L_i$	80	88	89.5
4	$\prod L_i$	84	90.5	92.5
5	$\sum I_i$	71	83	87
6	$\prod I_i$	84	90.5	93
7	$(\sum P_i + \sum L_i + \sum I_i) = \sum (P_i + L_i + I_i)$	85	94	94
8	$\prod P_i + \prod L_i + \prod I_i$	91	97	97
9	$\prod (P + L + I)_i$	90	95.5	96.5
10	$\sum P_i * \sum L_i * \sum I_i$	86.5	94.5	95.5
11	$\sum (P * L * I)_i$	79.5	91.5	94.5
12	$\prod P_i * \prod L_i * \prod I_i = \prod (P * L * I)_i$	93.5	97.5	98
13	$(\sum P_i + \sum L_i) * \sum I_i$	81	90	92
14	$\sum (P_i + L_i) * I_i$	73.5	82	85.5
15	$(\prod P_i + \prod L_i) * \prod I_i$	89	95	97
16	$\prod (P_i + L_i) * I_i$	88.5	94	95.5
17	$(\sum P_i + \sum I_i) * \sum L_i$	90	96	97
18	$\sum (P_i + I_i) * L_i$	91	96	97
19	$(\prod P_i + \prod I_i) * \prod L_i$	94	97.5	98
20	$\prod (\mathbf{P_i + I_i}) * \mathbf{L_i}$	**94.5**	**97.5**	**98**
21	$(\sum L_i + \sum I_i) * \sum P_i$	85	94	94
22	$\sum (L_i + I_i) * P_i$	92	93.5	94
23	$(\prod L_i + \prod I_i) * \prod P_i$	92	96.5	97
24	$\prod (L_i + I_i) * P_i$	94.5	95	96

the test data acquired during second phase. In our experiments, we computed separate subspace for each of the four fingers. This resulted in 12 subspaces and is judicious as the texture

patterns employed from four fingers are different. In our experiments, all the eigenvectors corresponding to the non-zero eigenvalues (401 in our case) were retained for the feature extraction. The number of eigenvectors employed LDA is (*r*-*n*) where *r* is the number of training samples and *n* represents the number of training classes. In ICA, a closed-form block source separation maximizing the contrast (2, 4), the sum of squares of fourth-order marginal cumulants for real data and mixtures is used [22]. We acquired two images from every user in the test phase and therefore 210 images are used for experiments. The number of clients in the experiments are 210 while the number of imposters in the experiments were 21840 (105×104×2). The receiver operating characteristics (ROC) illustrating the performance from different sub-space methods, on four knuckles, are shown in figure 13. The ROCs from individual knuckles suggests that PCA has performed better than LDA and ICA at lower FAR. The observed performance from the little finger knuckle is poorer than other three knuckles. The matching score combination from SUM and PROD rules has been most common in the literature [18]. Therefore ROC plots from these combinations using SUM and PROD rule are illustrated in figure 13-a. This figure also shows the ROC from the proposed product of sum rule which achieves better performance than conventional SUM or PROD rule.

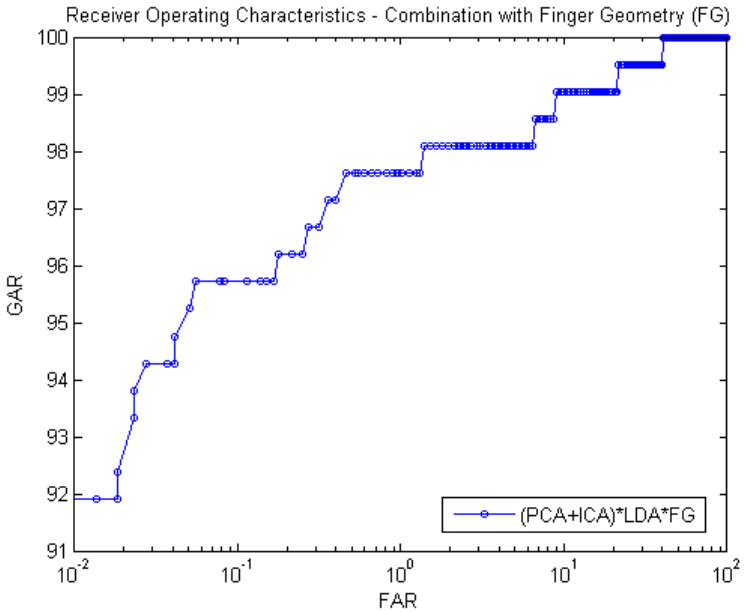

Figure 14: The ROC plots for combined performance from knuckles and finger geometry

The matching scores generated from PCA, LDA and ICA sub-space methods were analyzed individually and also for their rigorous combination. The table 1 presents summary of these experiments where *i* (1, 2, 3, and 4) represents the four different knuckles. The various combinations for matching scores from four extracted knuckles corresponding to the three sub-space methods are investigated. The 20th combination in this table, *i.e.* $\prod (P_i + I_i) * L_i$, achieves the best performance among all the combinations investigated. It performs better than all other combinations especially at lower FAR in table 1. The ROC corresponding to this combination is shown in figure 13(a). The figure 13-b shows the ROC plots obtained from the finger geometry features. The finger geometry features performed better as compared with the individual finger knuckles.

The matching scores generated from the finger geometry features were further combined with the best combination of three sub-space methods considered in this work. The ROC plot from this combination is shown in figure 14. The comparison of this plot with those in figure 13-a suggests that the combination of finger geometry features has been effective in achieving further performance improvement. The distribution of genuine and imposter matching scores from this combination is shown in figure 15. This distribution (histogram) is

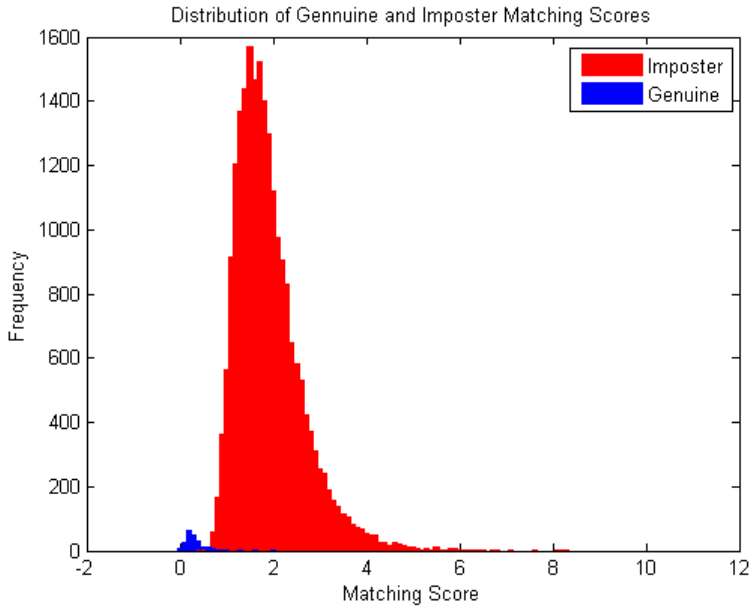

Figure 15: The Distribution of genuine and imposter matching scores

Table 2: Performance indices from the experiments

Analysis	EER (%)	Decidability Index
PCA	3.97	2.22
LDA	5.81	2.19
ICA	4.94	2.11
PCA+LDA+ICA	2.95	2.44
PCA*LDA*ICA	2.59	1.38
(PCA+ICA)*LDA	1.95	2.09
(PCA+ICA)*LDA*FG	1.39	2.35

quite similar to the Gaussian distribution and therefore the Decidability Index (*DI*) can also be used to ascertain the performance.

$$DI = \frac{\left|\mu_g - \mu_i\right|}{\sqrt{\sigma_g^2 + \sigma_i^2}} \tag{10}$$

where μ_g and μ_i are the mean while σ_g and σ_i are the variances of the genuine and imposter matching scores respectively [34]. The equal error rate (*EER*) and *DI* from the experimental results, corresponding to the best combinations in table 1, are summarized in table 2. Our experimental results illustrate that the combination (PCA+ICA)*LDA*FG achieves the best performance with EER of 1.39 and *DI* of 2.35.

7.1 Discussion

The experimental results shown in figure 13-a illustrate considerable improvement in the performance while consolidating the matching scores using fixed combination rules. The proposed POS scheme performed better than other combination schemes investigated (table 1) in our work. The SUM rule has been shown [27]-[28] to be useful for combining matching scores from the correlated feature spaces in which case the errors from the classifiers are independent. Thus the prior conclusions on the usage of SUM rule makes it most suitable for combining PCA- and ICA-based features as both of these sub-space methods employ natural

appearance based features of images and does not exploit class-dependent information. However, the LDA extracts features based on the class separability criterion estimated over the learning set and thus the features are highly class-dependent, as compared to those from PCA- and ICA-based features, and thus the PROD rule is argued to gain maximally on the assumption of independence in data representation. This could be a plausible explanation for the better performance of POS rule observed from the experiments. Furthermore, the knuckle texture from four fingers are observed to be highly independent and therefore the product of consolidated matching scores from each of the knuckles, generated from POS combination, is expected to perform better as also observed from the experimental results. The performance from little finger knuckle texture is poor as compared with those from other finger knuckles. This could be possibly due to its small image size and extended distance between the camera and little finger, especially during high rotation that also generates some distortion in the extracted little finger knuckle image (figure 10). The motivation behind employing only the knuckle region for identification, as compared to the larger finger surface, is that knuckle region presents most discriminative texture patterns that can be conveniently identified in the low resolution finger images. The remaining finger region is often obscured by hairs which makes the extraction of stable features extremely difficult.

Table 3: Typical computational timing for key processes

Process	**Time (msec)**
Image Loading	130
Image Binarization	20
Locating Contour Points	10
Finger Geometry Parameters	0.8
Knuckle Extraction (from all four fingers)	370

The proposed system was entirely implemented in C++ using the OpenCV [31] library. The

computational complexity of the key processes is summarized in table 3. The processes are run on Intel Pentium (4) CPU 3.00 GHz processor, with 1.97GB of RAM, and used GNU C++ compiler for the compilation. It can be observed from this table that the automated knuckle ROI extraction is the most computationally expensive operation. However, little time is required in the estimation of finger geometry features. In order to reduce computational complexity, two knuckle regions can be employed for feature extraction rather than all the four knuckles, preferably the ring and the middle finger knuckles as they achieve better performance (figure 12). The image loading (acquisition) time is considerable and can be significantly reduced by employing multi-threaded implementation.

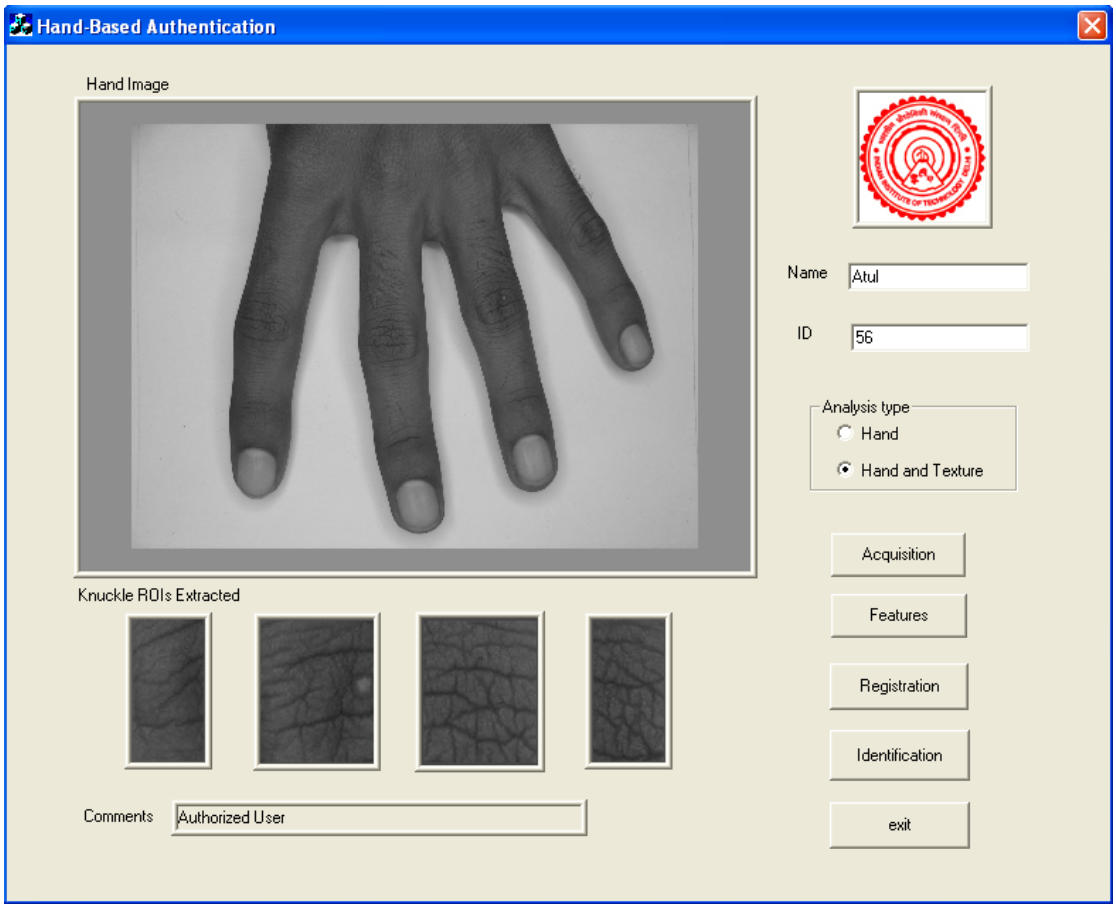

Figure 16: User authentication using graphical user interface

8. Conclusions

This paper has presented a new approach for personal authentication using finger back surface.

The developed system automatically extracts the knuckle texture and simultaneously acquires finger geometry features to reliably authenticate the users. The proposed method of knuckle region segmentation, finger ring detection, and the extraction of finger geometry features has been quite effective in achieving higher performance. The system is rigorously experimented on specially acquired finger-back image database from 105 users and achieved promising results. The experimental results presented in section 7 should be interpreted in view of the peg-free imaging setup as such images present significantly higher image variations as compared to those employing user-pegs to restrict the hand movement. The appearance-based features are extracted from the segmented knuckles using sub-space methods and a comparative study is reported. The computational analysis of the implemented modules presented in section 7.1 illustrates the suitability of the approach for online authentication. The graphical user interface (figure 16) allows user-friendly and easy access to the developed modules of the system for user authentication.

The palmprint and fingerprint features can be simultaneously extracted from the palm side hand images and combined to achieve the performance improvement [19], [30]. However, the size of finger knuckle is very small as compared with the palmprint and offers more attractive alternative as it also requires less processing as compared to palmprint. Therefore the finger knuckle features can be simultaneously[†] acquired along with the fingerprint features and combined to further improve the performance. The performance of the proposed authentication scheme highly depends on the accuracy of knuckle segmentation from the presented hands. Therefore further performance improvement can be achieved with the development of more accurate knuckle segmentation, which can also be achieved from some tradeoff in user convenience by employing user pegs (as in [2]) during imaging. It should be noted that the deformations generated in the knuckle texture due to variations in the finger bending and due

[†] The finger knuckles are invariably presented for identification on finger surface which is opposite to the fingerprint imaging surface.

to some disease, *e.g*. diabetes [37], are likely to degrade the performance and requires further investigation. In this work we acquired a medium size database for performance evaluation of the proposed scheme. However, in the near future we plan to acquire a large scale database of the order of 500 to 1000 users for further research and performance evaluation. *Although more work remains to be done, our results to date indicate that the combination of finger-knuckle and finger-geometry features constitutes a promising addition to the hand-based personal authentication systems.*

9. References

1. P. H. Hennings-Yeomans, B. V. K. Kumar, and M. Savvides, "Palmprint classification using multiple advanced correlation filters and palm-specific segmentation," *IEEE Trans. Information Forensics and Security*, vol. 2, no. 3, pp. 613-622, Sep. 2007.

2. D. Zhang, W. K. Kong, J. You, and M. Wong, "On-line palmprint identification," *IEEE Trans. Pattern Analysis and Machine Intelligence*, vol. 25, pp. 1041-1050, Sep. 2003.

3. A. K. Jain, A. Ross, and S. Pankanti, "A Prototype hand geometry-based verification system", *Proc. of 2nd International Conference on Audio and Video-Based Biometric Person Authentication*, Washington DC, pp.166-171, Mar.1999.

4. A. Kumar and D. Zhang, "Personal recognition using hand shape and texture", *IEEE Trans. Image Processing*, vol. 15, no. 8, pp. 2454- 2461, 2006.

5. S. Ribaric, and I. Fratric, "A Biometric Identification System Based on Eigenpalm and Eigenfinger Features," *IEEE Trans. Pattern Analysis and Machine Intelligence*, vol.27, no.11, Nov. 2005.

6. X. Lu, D. Zhang, and K. Wang, "Fisherpalms based palmprint recognition," *Pattern Recognition Letters*, vol. 24, pp. 2829-2838, Nov. 2003.

7. A. Kumar and D. Zhang, "Hand geometry recognition using entropy-based discretization," *IEEE Trans. Information Forensics and Security*, vol. 2, pp. 181-187, Jun. 2007.

8. Sanchez Paper HG R. Sanchez-Reillo, C. Sanchez-Avila, and A. Gonzalez-Macros, "Biometric Identification through Hand Geometry Measurements", *IEEE Trans. Pattern Analysis and Machine Intelligence,* vol.22, no.10, pp. 1168-1171, Oct. 2000.

9. D. L. Woodard, P. J. Flynn, "Finger surface as a biometric identifier", *Computer Vision and Image Understanding*, pp. 357-384, vol. 100, Aug. 2005.

10. S. Malassiotis, N. Aifanti, and M. G. Strintzis, "Personal Authentication using 3-D finger geometry", *IEEE Trans. Information Forensics and Security*, vol.1, no.1, pp.12-21, Mar. 2006.

11. J.-G. Wang, W.-Y. Yau, A. Suwandy, and E. Sung, "Person recognition by fusing palmprint and palm vein images based on "Lapacianpalm" representation," *Pattern Recognition*, vol. 41, pp. 1531-1544, 2008.

12. A. Kumar and K. V. Prathyusha, "Personal authentication using hand vein triangulation," *Proc. SPIE Biometric Technology for human identification*, vol. 6944, Orlando, pp. 69440E-69440E-13, Mar. 2008
13. C.-L. Lin and K.-C. Fan, "Biometric Verification Using Thermal Images of Palm-Dorsa Vein Patterns" *IEEE Trans. Circuits & Sys. for Video Technology*, vol. 14, pp. 199 – 213, Feb. 2004.
14. A. Kumar and D. Zhang, "Personal Authentication using multiple palmprint representation," *Pattern Recognition*, vol. 38, pp. 1695-1704, Mar. 2005.
15. Z. Sun, T. Tan, Y. Yang, and S. Z. Li, "Ordinal palmprint representation for personal identification," *Proc. CVPR 2005*, pp. 279-284, 2005.
16. X. Jiang, W. Xu, L. Sweeney, Y. Li, R. Gross, and D. Yurovsky, "New directions in contact free hand recognition," *Proc. ICIP 2007*, pp. 389-392, 2007.
17. N. Otsu, "A threshold selection method from gray-level histograms", *IEEE Trans. Systems, Man and Cybernetics*, vol. 9, no. 1, pp. 62-66, 1979.
18. Handbook of Multibiometrics, *A. Ross, K. Nandakumar*, and *A. K. Jain*, Springer, 2006.
19. A. Kumar and D. Zhang, "Combining fingerprint, palmprint and hand-shape for user authentication," *Proc. ICPR 2006*, pp. 549-552, Hong Kong, Aug, 2006.
20. B. A. Draper, K. Baek, M. S. Bartlett, and J. R. Beveridge, "Recognizing faces with PCA and ICA," *Computer Vision and Image Understanding*, vol. 91, pp. 115-137, July 2003.
21. C. Havran, L. Hupet, J. Czyz, J. Lee, L. Vandendorpe, and M. Verleysen, " Independent Component Analysis for face authentication", *Proc. KES*, *Knowledge Based Intelligent Information and Engineering Systems,* Crema (Italy), pp. 1207-1211, Sep., 2002.
22. A. Hyvärinen, "Fast and robust fixed-point algorithms for independent component analysis," *IEEE Trans. Neural Networks*, vol. 10, no. 3, pp. 626-634, May 1999.
23. Y. Wang and J. Qiang Han, "Iris Recognition using Independent Component Analysis", *Proc. of 4th Intl. Conference on Machine Learning and Cybernetics,* Guangzhou, vol. 7, pp. 4487-4492, Aug., 2005.
24. X. Lu, Y. Wang, and A. K. Jain, "Combining classifiers for face recognition", *Proc. ICME*, vol. 3, pp.13-16, Jul. 2003.
25. G. L. Marcialis and F. Roli, "Fusion of LDA and PCA for Face Verification", *Proc. ECCV Workshop Biometric Authentication*, pp. 30-38, 2002.
26. J. Yi, J. Kim, J. Choi, J. Han and E. Lee, "Face Recognition based on ICA combined with FLD", *Proc. ECCV Workshop Biometric Authentication*, pp. 10-18, 2002.
27. D. M. J. Tax, M. V. Breukelen, R. P. W. Duin, and J. Kittler, "Combining multiple classifiers by averaging or multiplying," *Pattern Recognition*, vol. 33, pp. 1475-1485, 2000.
28. D. M. J. Tax, R. P. W. Duin, and M. van Breukelen, "Comparison between product and mean classifier combination rules," *Proc. First Intl. workshop on Statistical Techniques in Pattern Recognition*, Institute of Information Theory and Automation, pp. 165-170, Jun. 1997.
29. http://www.solitontech.com/products_machine_vision_cameras.htm
30. R. K. Rowe, U. Uludag, M. Demirkus, S. Parthasaradhi and A. K. Jain, "A multispectral whole-hand biometric authentication system," *Proc. Biometric Symposium*, Baltimore, Sep. 2007.

31. http://sourceforge.net/projects/opencvlibrary

32. K. Okada, J. Steffens, T. Maurer, H. Hong, E. Elagin, H. Neven, and C. von der Malsburg, "The Bochum/USC face recognition system and how it fared in the FERET phase III test," *Face Recognition: From Theory to Applications*, H. Wechsler, P.J. Phillips, V. Bruce, F.F. Soulie and T.S. Huang (Eds.), Springer-Verlag, pp. 186-205, 1998.

33. http://www.cis.hut.fi/projects/ica/fastica

34. Biometric Systems: Technology, Design and Performance Evaluation, *J. Wayman, A. K. Jain, D. Maltoni, and D. Maio* (*Eds*), Springer, 2005.

35. S. Ribaric and I. Fratric, "An online biometric authentication system based on eigenfingers and finger-geometry," *Proc. 13th European Signal Processing Conf.*, Antalya, Turkey, Sep. 2005.

36. A. Hyvärinen, J. Karhunen, and E. Oja, *Independent Component Analysis*, John Wiley, 2001.

37. C. Guarneri, F. Guarneri, F. Borgia, and M. Vaccaro, "Finger pebbles in a diabetic patient: Huntley's papules," *Int. J. Dermatology*, vol. 44, issue 9, pp. 755-756, Dec. 2004.

38. A. Kumar, "Incorporating cohort information for reliable palmprint authentication," *Proc. 6th Indian Conf. Computer Vision, Graphics, and Image Processing*, Bhubaneswar, India, Dec. 2008, pp. 583–590. 2008.